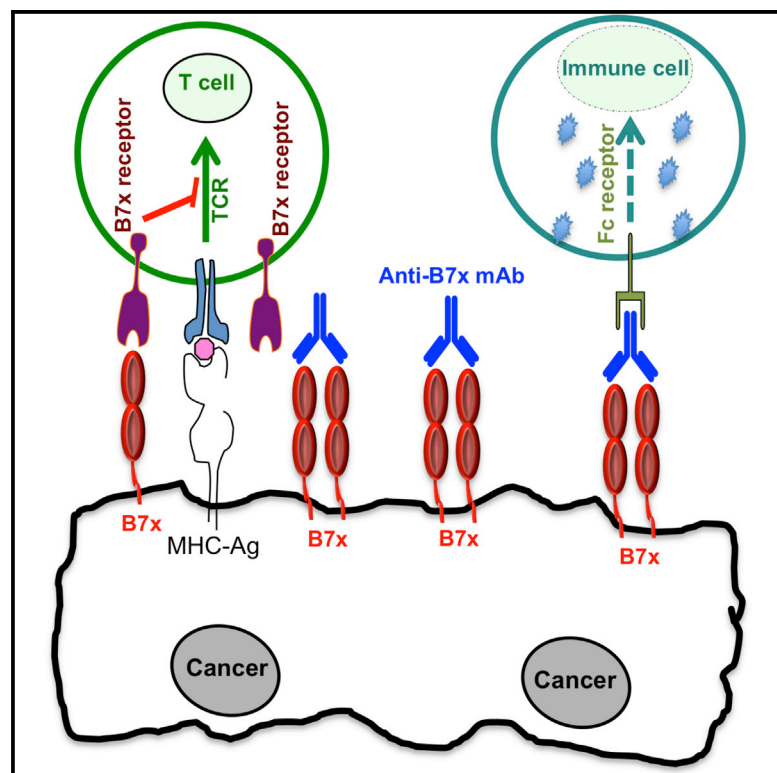Article

Structure and Cancer Immunotherapy of the B7 Family Member B7x

Graphical Abstract

Authors

Hyungjun Jeon, Vladimir Vigdorovich, ...,
Steven C. Almo, Xingxing Zang

Correspondence

steve.almo@einstein.yu.edu (S.C.A.),
xing-xing.zang@einstein.yu.edu (X.Z.)

In Brief

B7x is an attractive therapeutic target for cancer immunotherapy. Jeon et al. now develop an in vivo screening system to find therapeutic monoclonal antibodies (mAbs) that target B7x on tumors. The mAb 1H3 is able to significantly inhibit growth of B7x-expressing tumors in vivo through multiple mechanisms.

Highlights

The crystal structure of the human B7x IgV domain is determined

An in vivo system is developed to screen therapeutic mAbs against B7x

mAb 1H3 treatment suppresses tumor growth and prolongs survival in tumor models

Anti-B7x immunotherapy creates an environment with enhanced antitumor immunity

Accession Numbers

4GOS

CrossMark

CellPress

Structure and Cancer Immunotherapy of the B7 Family Member B7x

Hyungjun Jeon,[1,5] Vladimir Vigdorovich,[1,5,6] Sarah C. Garrett-Thomson,[2] Murali Janakiram,[3] Udupi A. Ramagopal,[2] Yael M. Abadi,[1,7] Jun Sik Lee,[1,8] Lisa Scandiuzzi,[1] Kim C. Ohaegbulam,[1] Jordan M. Chinai,[1] Ruihua Zhao,[1,9] Yu Yao,[4] Ying Mao,[4] Joseph A. Sparano,[3] Steven C. Almo,[2,*] and Xingxing Zang[1,3,*]

[1]Department of Microbiology and Immunology, Albert Einstein College of Medicine, Bronx, NY 10461, USA
[2]Department of Biochemistry, Physiology and Biophysics, Albert Einstein College of Medicine, Bronx, NY 10461, USA
[3]Department of Oncology, Montefiore Medical Center, Albert Einstein College of Medicine, Bronx, NY 10467, USA
[4]Department of Neurosurgery, Huashan Hospital, Fudan University, Shanghai 200040, China
[5]Co-first author
[6]Present address: Seattle BioMed, Seattle, WA 98109, USA
[7]Present address: Department of Neurology, Yale University School of Medicine, New Haven, CT 06510, USA
[8]Present address: Department of Biology, College of Natural Science, Chosun, University, Gwangju 501-759, South Korea
[9]Present address: School of Life Science, Fudan University, Shanghai 200433, China
*Correspondence: steve.almo@einstein.yu.edu (S.C.A.), xing-xing.zang@einstein.yu.edu (X.Z.)
http://dx.doi.org/10.1016/j.celrep.2014.09.053

SUMMARY

B7x (B7-H4 or B7S1) is a member of the B7 family that can inhibit T cell function. B7x protein is absent in most normal human tissues and immune cells, but it is overexpressed in human cancers and often correlates with negative clinical outcome. The expression pattern and function of B7x suggest that it may be a potent immunosuppressive pathway in human cancers. Here, we determined the crystal structure of the human B7x immunoglobulin variable (IgV) domain at 1.59 Å resolution and mapped the epitopes recognized by monoclonal antibodies. We developed an in vivo system to screen therapeutic monoclonal antibodies against B7x and found that the clone 1H3 significantly inhibited growth of B7x-expressing tumors in vivo via multiple mechanisms. Furthermore, the surviving mice given 1H3 treatment were resistant to tumor rechallenge. Our data suggest that targeting B7x on tumors is a promising cancer immunotherapy and humanized 1H3 may be efficacious for immunotherapy of human cancers.

INTRODUCTION

T cell costimulation and coinhibition mediated by the B7 ligand family and the CD28 receptor family have crucial roles in modulating T cell activation, proliferation, and differentiation into effector function and memory generation (Greenwald et al., 2005; Zang and Allison, 2007). The B7-1/B7-2/CD28/CTLA-4 pathway is a well-characterized T cell costimulatory and coinhibitory pathway. A monoclonal antibody (mAb) against CTLA-4 was recently approved for the treatment of metastatic melanoma (Hodi et al., 2010; Sharma et al., 2011), and CTLA-4-Ig fusion protein has been used to treat rheumatoid arthritis and prevent acute kidney transplant rejection (Fiocco et al., 2008; Vincenti

et al., 2011). The past decade has witnessed a new era in the discovery of other B7 and CD28 members and understanding of their immune regulation, including B7h/ICOS, PD-L1/PD-L2/PD-1, B7-H3/receptor, B7x/receptor, and HHLA2 (B7y/B7-H5/B7h7)/TMIGD2 (CD28h) (data not shown; Zhao et al., 2013; Zhu et al., 2013). mAbs against PD-1 and PD-L1 are currently in clinical trials with cancer patients (Brahmer et al., 2012; Topalian et al., 2012). Clearly, further studies of the less characterized B7/CD28 pathways will not only sharpen our understanding of the immune system but also lead to new therapies for a wide range of diseases.

B7x (B7-H4 or B7S1), a member of the B7 family, can inhibit T cell proliferation and cytokine production in vitro (Prasad et al., 2003; Sica et al., 2003; Zang et al., 2003). Recent studies reveal that overexpression of B7x on pancreatic cells is sufficient to abolish CD4 or CD8 T cell-induced diabetes (Lee et al., 2012; Wei et al., 2011), demonstrating that manipulating the B7x pathway can achieve significant functional consequences in vivo. In contrast to the expression pattern of B7-1 and B7-2, B7x protein is mainly detected in nonlymphoid organs (Hofmeyer et al., 2012; Lee et al., 2012; Tringler et al., 2005; Wei et al., 2011). One of the most intriguing characteristics of B7x is that it is overexpressed in numerous human cancers and, in many cases, correlates with negative clinical outcome (Barach et al., 2011; Janakiram et al., 2012; Zang and Allison, 2007). A large investigation of B7 family molecules in human malignancy demonstrated that prostate cancer patients with tumors that express B7x highly are more likely to have disease spread at the time of surgery and are at an increased risk of cancer recurrence and cancer-specific death (Zang et al., 2007). In another study, 103 ovarian cancer samples tested expressed B7x (Zang et al., 2010). In contrast to tumor tissues, only scattered B7x-positive cells are detected in nonneoplastic ovarian tissues (Zang et al., 2010). In line with these results, others have reported that B7x overexpression can be seen in human cancers of the lung (Sun et al., 2006), breast (Tringler et al., 2005), kidney (Krambeck et al., 2006), pancreas (Awadallah et al., 2008), esophagus (Chen et al., 2011), skin (Quandt et al., 2011), and gut (Jiang et al.,

Table 1. Data Collection, Phasing, and Refinement Statistics for SAD

Data Collection	Native	I3C
Space group	P $4_3 2_1 2$	P $4_3 2_1 2$
Cell dimensions		
α, β, γ (Å)	46.5, 46.5, 115.77	46.47, 46.47, 116.15
a, b, g (°)	90, 90, 90	90, 90, 90
Wavelength	1.075	1.5402
Resolution (Å)	43.1–1.59	38.72–1.79
R_{sym} or R_{merge}	8.8 (48.9)	16.1 (179)
I/σI	17.7 (1.6)	13.8 (1.8)
Completeness (%)	90.1 (100.0)	86.4 (89.4)
Redundancy	13.3 (13.5)	18.4 (19.7)
Refinement		
Resolution (Å)	1.59	
No. reflections	15,194	
R_{work}/R_{free}	17.4 (23.2)/19.2 (22.6)	
No. of atoms		
Protein	871	
Ligand/ion	61	
Water	111	
B-factors		
Protein	15.0	
Ligand/ion	13.8	
Water	24.1	
Rmsd		
Bond lengths (Å)	0.009	
Bond angles (°)	1.474	

One crystal was used for native and one for I3C-derivatized data sets. Values in parentheses are for the highest-resolution shell.

2010). In renal cell carcinoma (Krambeck et al., 2006), patients with tumors expressing B7x are three times more likely to die of cancer compared to patients lacking B7x. In esophageal squamous cell carcinoma, expression levels of B7x on tumor cells are significantly correlated with distant metastasis, tumor stage and worse survival and are inversely correlated with densities of CD3 T cells in tumor nest and CD8 T cells in tumor stroma (Chen et al., 2011).

The overexpression of B7x by so many types of human cancers suggests that this pathway may be exploited as an important immune-evasion mechanism. Here, we report the first crystal structure of the human B7x immunoglobulin variable (IgV) domain and developed a cancer immunotherapy using mAbs recognizing this domain. Our findings suggest that targeting B7x on tumors can be an innovative tumor immunotherapy.

RESULTS

Crystal Structure of the Human B7x IgV Domain

Like other B7 family members, B7x possesses extracellular IgV and immunoglobulin constant (IgC) domains (Prasad et al., 2003; Sica et al., 2003; Zang et al., 2003). The IgV domain has previously been characterized as the receptor-binding domain for B7-1 (Stamper et al., 2001), B7-2 (Schwartz et al., 2001), PD-L1 (Lin et al., 2008), and PD-L2 (Lázár-Molnár et al., 2008). Therefore, we sought to understand the structure of the B7x IgV domain (B7x-IgV) to inform future studies of its interaction with receptors and antibodies. Human and murine B7x sequences share ~90% sequence identity overall and in their IgV domains. The crystals of human B7x-IgV exhibited diffraction consistent with the space group P$4_3 2_1 2$ (a = 46.5 Å, b = 46.5 Å, c = 115.77 Å; one molecule per asymmetric unit) and extended to 1.59 Å (Table 1). The final model consists of residues 35–148, which are organized into a β sandwich composed of sheets ABED (back-sheet; light blue) and C′′C′CFG (front-sheet; light green) (Figure 1A). The sequence of the human B7x-IgV is predicted to contain a single glycosylation site at Asn112, and we observed a region of well-defined electron density near this position consistent with the presence of corresponding to five sugar residues of a branched glycan (Figure 1B). Superposition of B7x and PD-L1 IgV domains (Figure 1C) resulted in a root-mean-square deviation (rmsd) of 1.327 Å with differences apparent largely in the loop regions, demonstrating that the fold is highly conserved between these two B7 family members.

Interaction of mAbs with the B7x IgV Domain

We recently generated B7x-specific mAbs from B7x$^{-/-}$ mice (Wei et al., 2011). mAbs 1H3 (immunoglobulin G1 [IgG1]) and 12D11 (IgG1) bound human or mouse B7x, but not other B7 family members (Figure S1A). We estimated the binding rate constants and derived the corresponding equilibrium dissociation constants (K_D's) for the interactions of mAbs with recombinant murine B7x ectodomain, as well as murine and human B7x IgV through surface plasmon resonance (SPR). In these experiments, purified antibodies were immobilized on the biosensor surface and recombinant protein samples at various concentrations were injected for 120–240 s followed by dissociation in running buffer. mAbs 1H3, 12D11, and 15D12 strongly interacted with all of these proteins, and dissociation constants are summarized in Table 2. Representative sensorgrams are shown in Figure S1B.

Mapping the Epitopes in the Human B7x IgV Domain Recognized by 1H3 and 12D11

To define the epitope recognized by 1H3 and 12D11, we generated a series of B7x point mutants and measured their effect on binding of 1H3 and 12D11. Both antibodies showed a similar pattern of binding to B7x except in the case of the I62A mutant. Mutations at residues E59, I62, K63, E74, K84, F104, D106, Q107, and S135 resulted in greater than 40% loss of antibody binding (Figure 1D; Figure S1C), even though their overall expression was similar to wild-type B7x. These observations suggest that perturbation of these residues did not cause global B7x misfolding or instability and that the effects on antibody binding were the result of impaired/unfavorable interactions at the binding interface. Clustering of the identified residues on the surface of the B7x IgV domain further suggests that the observed effects on antibody binding were not due to nonspecific effects on overall structure or stability of B7x.
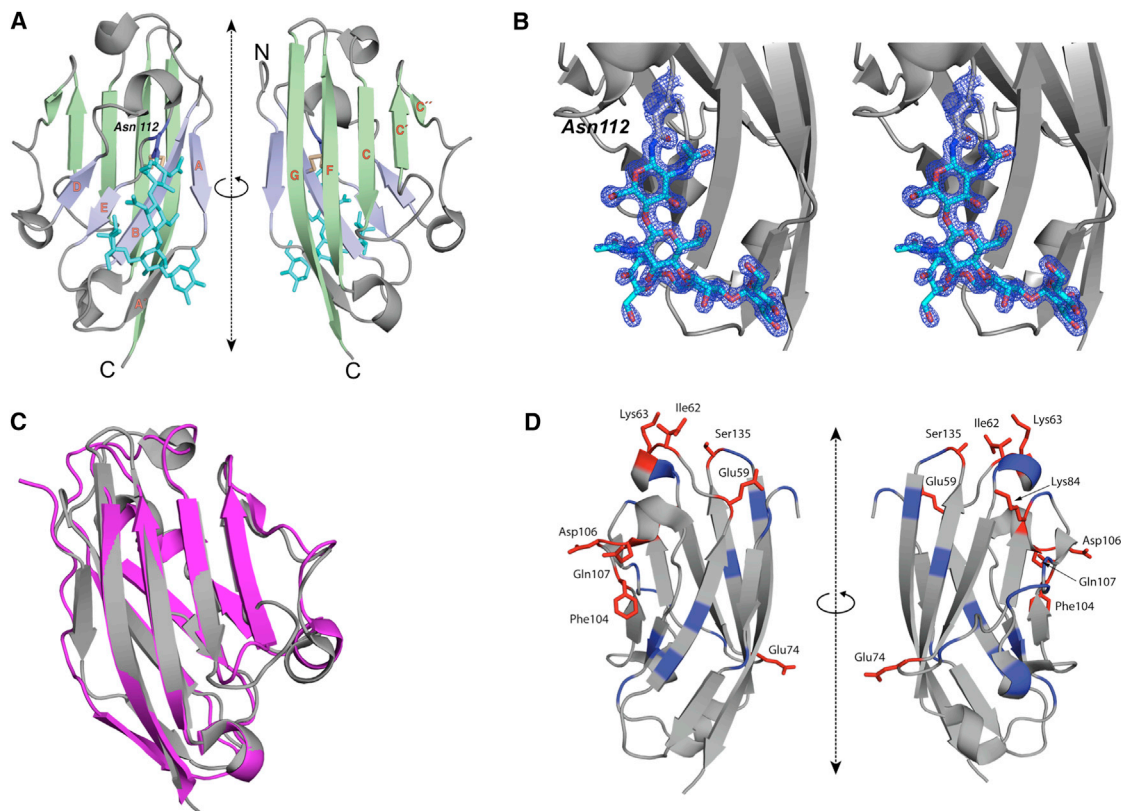
Figure 1. The Structure of the Human B7x IgV Domain and the Epitopes Recognized by Monoclonal Antibody against B7x

(A) Ribbon representation of the structure of human B7x-IgV (front sheet, light green; back sheet, light purple; disulfide, light yellow) is shown in two orientations. The strands of the β sandwich are labeled in orange; the side chain of Asn112 (purple) and the N-linked glycan (cyan) are shown in stick-figure representation.

(B) Electron density observed near Asn112 corresponds to an N-linked glycan. Ribbon representation of the structure of human B7x-IgV (gray) is shown. Electron density map ($2F_o - F_c$), contoured at $+2\sigma$, and covering the area near and including Asn112 is shown in mesh representation (blue). The five residues of N-linked glycan are shown in stick representation.

(C) Superposition of B7x and PD-L1. Gray represents the IgV domain of human PD-L1, and Pink represents the IgV domain of human B7x.

(D) Ribbon diagram of the IgV domain of B7x showing the location of residues targeted for mutagenesis. Positions that when mutated resulted in at least 40% reduction in 1H3 binding are highlighted in red, while the remainder of targeted positions are highlighted in blue.

Anti-B7x mAb Therapy in Mouse B7x-Expressing Tumor Models

Although B7x is overexpressed in many human cancers (Jeon et al., 2013), it is lost rapidly in vitro culture (Dangaj et al., 2013). We found that most human and mouse tumor cell lines were B7x protein negative. To develop a functional screening system for immunotherapy, we first established tumor cell lines that stably express cell-surface B7x using a retroviral expression vector transfection. (Figures S2A and S2B). The B7x expression level on CT26 cells was comparable to the expression levels of B7x on human cancer cell lines such as MCF-7, MDA-MB-468, and SK-BR-3 (Figures S2C–S2E). Mouse colon carcinoma CT26 and murine and human B7x/CT26 were intravenously (i.v.) injected into syngeneic BALB/c mice to induce experimental lung metastasis. The average number of lung tumor nodules in murine and human B7x/CT26 group was ~3.5-fold higher than that in the CT26 group (Figure S2F). In line with this result, B7x/CT26-injected mice had a lower survival rate compared to mice receiving naive CT26 cells (Figure S2G).

These results demonstrate that B7x overexpression on a murine tumor cell line, like on human tumors, correlates with worse outcomes.

We next screened the in vivo therapeutic effect of B7x-specific mAbs in the B7x/CT26-induced pulmonary metastasis model. B7x/CT26 cells were i.v. injected into BALB/c mice followed by intraperitoneal (i.p.) injection of anti-B7x mAbs. On day 17, lung tumor nodules were examined. We found that two mAbs, 1H3 and 12D11, significantly reduced ~60% of tumor nodules in lungs (Figure 2A). The 4T1 murine tumor model is a widely used model in which the cancerous cells spontaneously metastasize to the lung (Aslakson and Miller, 1992). We then decided to validate the efficacy of 1H3 in the murine B7x/4T1 primary tumor model (Figure S2H). 1H3 treatment significantly suppressed primary tumor growth and efficiently reduced primary tumor-induced metastatic tumor nodules in the lung (Figures 2B and S4B). These results from two tumor models suggest that anti-B7x markedly reduces tumor nodules in lungs.

Table 2. Surface Plasmon Resonance Measurements

mAb	k_{on} (M$^{-1}\cdot$s^{-1})	k_{off} (s^{-1})	K_D (nM)
Murine B7x (IgV Domain)			
1H3	$2.455(4) \times 10^6$	0.001248(7)	0.508(3)
12D11	$2.140(4) \times 10^6$	0.001341(8)	0.627(4)
15D12	$1.790(3) \times 10^6$	0.001135(7)	0.634(4)
Murine B7x			
1H3	$6.71(3) \times 10^5$	0.001298(7)	1.94(1)
12D11	$6.62(4) \times 10^5$	0.001177(7)	1.78(1)
15D12	$4.40(3) \times 10^5$	0.001095(6)	2.49(2)
Human B7x (IgV Domain)			
1H3	$2.53(2) \times 10^5$	0.00917(4)	36.2(3)
12D11	$2.13(1) \times 10^5$	0.00928(3)	43.5(3)
15D12	$1.388(7) \times 10^5$	0.01039(2)	74.9(4)

The value in parentheses denotes the SE in the last digit.

Anti-B7x mAb Therapy in a Human B7x-Expressing Tumor Model

B7x is very evolutionarily conserved (Prasad et al., 2003; Sica et al., 2003; Zang et al., 2003), and mature B7x protein shares 90% amino acid identity in the extracellular domains between human and mice. Since both 1H3 and 12D11 recognized human B7x (Table 2), we wanted to test the therapeutic effects of these two mAbs in a human B7x-expressing tumor model in vivo. Like mouse B7x, the expression of human B7x on CT26 markedly increased tumor nodules in the lung (Figure S2F). We then examined the effect of mAbs on hB7x/CT26 in vivo. Mice were i.v. injected with hB7x/CT26 and then treated with 1H3 or 12D11. On day 17, the average numbers of lung tumor nodules in 1H3-treated and 12D11-treated groups were 97 and 236, respectively, whereas the number in the control group was 251 (Figure 2C). Because proteins in the tumor microenvironments can be modified by posttranslational modifications such as glycosylation and phosphorylation, we questioned whether 1H3 recognized human B7x that is naturally expressed in human tumors. Using immunohistochemical staining, we found that 1H3 recognized nature B7x in various human cancers from the colon, ovary, skin, lung, breast, liver, nasal cavity, liposarcoma, pancreas, and stomach (Figure 2D). These results suggest that human B7x promotes tumor growth in vivo and that mAb 1H3 recognizes human B7x and inhibits progression of these tumors in vivo. As 1H3 was the only mAb that inhibited both human and mouse B7x-mediated tumor progression, we used it for the subsequent experiments.

1H3 mAb-Treated Mice Survive Tumor Rechallenge

We next investigated the effect of 1H3 on the survival of mice bearing B7x/CT26 tumor. In agreement with the lung tumor nodule results, 1H3-treated mice had a significant lower mortality than did control immunoglobulin G (IgG)-treated mice. By day 60 postinjection of tumor, 100% of IgG-treated mice were dead, whereas only 50% of 1H3-treated mice had died (Figure 3A). These surviving mice appeared to be healthy. We then examined whether the surviving mice had resistance to the tumor rechallenge. These mice were rechallenged with the same number of

B7x/CT26 cells, and all of them remained alive. On day 120, mice were sacrificed and their lungs were free of visible tumor nodules. Furthermore, hematoxylin and eosin (H&E) staining of lung sections from these mice showed that they were free of cancerous cells (Figure 3B).

Anti-B7x Therapy Increases Infiltrating T and NK Cells and Decreases Infiltrating MDSCs in Tumors

To dissect the therapeutic mechanisms of 1H3 treatment, we prepared single-cell suspensions from tumor-bearing lungs and analyzed the immune cells by flow cytometry. 1H3-treated mice had a significantly higher percentage of CD45$^+$ immune cell infiltrate than control IgG-treated mice (Figure 4A). Among these CD45$^+$ cells, the 1H3 treatment strongly increased tumor infiltrates of CD8 T cells and natural killer (NK) cells (Figure 4B), two major types of antitumor immune cells. We used SPSY-VYHQF/H-2L^d tetramer to detect CD8 T cells specific for CT26 tumor antigen epitope AH1 (amino acids 423–431 SPSY-VYHQF) (Huang et al., 1996). In agreement with the increased total CD8 T cells, 1H3 treatment increased the percentage of AH1-specific CD8 T cells (Figure 4C). In addition, we found that the percentage of AH1-specific CD8 T cells in the blood was reduced in 1H3-treated mice (Figure 4D), but the percentage of tumor-associated macrophages in the blood was not changed by 1H3 treatment (Figure S3A). There were no significant changes in AH1-specific CD8 T cells and tumor-associated macrophages in spleens. These results suggest that 1H3 treatment facilitated the migration of tumor-specific CD8 T cells from the blood to tumor-bearing lungs. Recent studies identified the coexpression of Tim-3 and PD-1 (Tim-3+PD-1+) cells as a unique phenotype of exhausted CD8 or CD4 T cells in melanoma and leukemia (Fourcade et al., 2010; Goding et al., 2013; Zhou et al., 2011). Therefore, we examined the effect of 1H3 on these two inhibitory receptors on T cells. We found that 1H3-treated mice had significantly fewer CD4 T cells that were Tim-3+PD-1+, Tim-3+ alone and PD-1+ alone relative to those of control mice (Figure 4E). These results suggest that 1H3 treatment reduced the conversion of CD4 T cells from an activated to an exhausted state. Along with these findings, 1H3 treatment enhanced CD4 T cells to produce interferon-γ (IFN-γ; Figure 4F), a critical cytokine for antitumor immunity. Perforin and granzyme B are effector molecules in CD8 T cells and NK cells that mediate tumor cell death. We found that 1H3 treatment increased their production in CD8 T cells and NK cells, although the difference did not reach statistical significance (Figures S3B and S3C). In the tumor microenvironment, suppression of effector T cell function is often driven by immunosuppressive cells. Therefore, we investigated the effect of 1H3 treatment on immunosuppressive cell infiltrates in tumor-bearing lungs. We found that the treatment did not change the percentage of Foxp3$^+$CD4$^+$ regulatory T cells (Tregs; Figure S3D), but it did reduce CD11b$^+$Ly6C$^+$ monocytic myeloid-derived suppressor cells (MDSCs) infiltrating the tumor (Figure 4G). The increase of CD8 T cells, NK cells, and IFN-γ-producing CD4 T cells combined with the reduction of MDSCs in the 1H3 treatment collectively creates an environment with a lower ratio of suppressive cells to antitumor effector cells (Figure 4H).
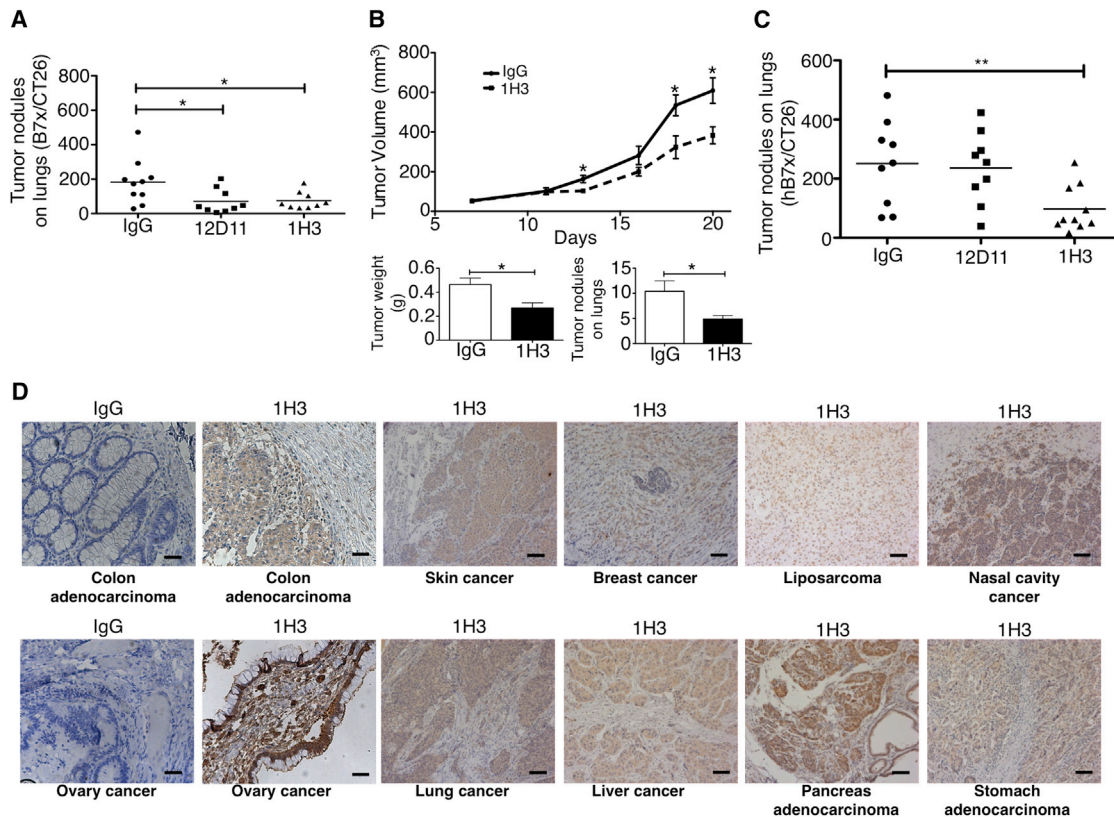
Figure 2. Effect of Anti-B7x Monoclonal Antibodies on Tumor Growth

(A) BALB/c mice were i.v. injected with B7x/CT26, then with anti-B7x mAbs 12D11 and 1H3 or mouse IgG. After sacrifice, tumor nodules in lungs were counted. Data were pooled from three independent experiments (n = 9 or 10).

(B) BALB/c females were injected with B7x/4T1 in the mammary fat pad. Mice were i.p. treated with mAb 1H3. Tumor volumes were measured every 2 or 3 days after tumor injection. After mice were sacrificed, tumor weights were measured and tumor nodules on lungs were counted (n = 10). *p < 0.05.

(C) BALB/c mice were i.v. injected with CT26 cells expressing human B7x (hB7x/CT26) and then injected i.p. with mAb 1H3 or control IgG. After sacrificing the mice, tumor nodules in the lungs were counted (n = 9). Results were pooled from two independent experiments.

(D) Several human cancers were stained with 1H3 or IgG control using immunohistochemistry. Scale bars, 50 μm.

Effect of Anti-B7x Therapy on the Tumor Microenvironment

Vascular endothelial growth factor (VEGF) from tumor cells, stromal cells, and immune cells stimulates angiogenesis in the tumor microenvironment. This angiogenesis facilitates tumor growth and metastasis (Roda et al., 2012; Roland et al., 2009). We found that the VEGF concentration in tumor-bearing lungs from 1H3-treated mice was significantly lower than that of control mice (Figure 4I). The 1H3 treatment also lowered the concentration of transforming growth factor β (TGF-β) in tumor-bearing lungs (Figure 4J), one of the key cytokines responsible for suppressing antitumor immunity (Fridlender et al., 2009).

1H3 Kills Tumor Cells through ADCC

Antibodies can eliminate virus-infected cells or tumor cells via antibody-dependent cellular cytotoxicity (ADCC) (Clynes et al., 2000; Isitman et al., 2012; Kohrt et al., 2012), a mechanism requiring antibody, antigen-expressed target cells, and effector cells expressing Fc receptors. We examined whether 1H3 was able to kill tumor cells expressing B7x or tumor cells without expressing B7x through ADCC. We found that 1H3 induced 50%

more target cells death compared to control IgG (Figures 5A and S4A).

1H3 Partially Blocks B7x-Mediated T Cell Coinhibition

It has been demonstrated that B7x inhibits T cell function in the presence of T cell receptor signaling in vitro (Prasad et al., 2003; Sica et al., 2003; Zang et al., 2003), but the receptor expressed on activated T cells is currently unknown. We next questioned whether 1H3 could inhibit B7x-mediated T cell coinhibition using a system modified from our previous studies (Zang et al., 2003). As expected, T cells proliferated vigorously when incubated with anti-CD3 and control immunoglobulin, with more than 73% of T cells dividing. When T cells were incubated with anti-CD3 and B7x-Ig, significantly fewer T cells proliferated, with about 41% dividing. The presence of 1H3 in the system significantly neutralized B7x-mediated T cell coinhibition, as 1H3 increased T cell proliferation to >61%. Furthermore, the Fab fragment of 1H3 had a similar neutralizing effect on B7x-induced T cell coinhibition (Figure 5B). These results reveal that 1H3 can partially block B7x-mediated T cell coinhibition. To assess whether 1H3 therapy depends on ADCC and/or functional neutralization
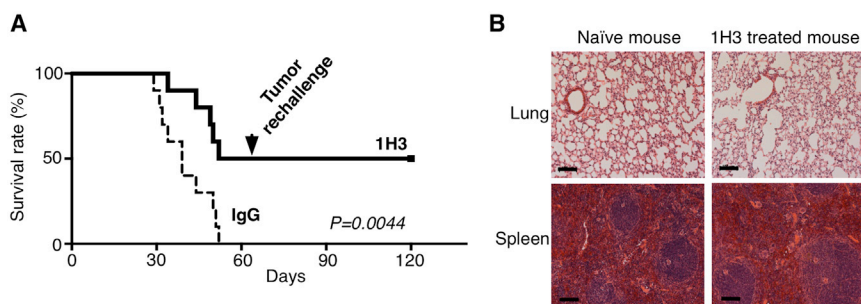
Figure 3. Effect of Anti-B7x Therapy on Survival and Tumor Rechallenge

(A) BALB/c mice were i.v. injected with B7x/CT26 at day 0 and then injected i.p. with 1H3 or control IgG. At day 60 postinjection, the surviving mice were i.v. rechallenged with B7x/CT26 (n = 10). *p < 0.05; **p < 0.01.

(B) At day 120, surviving mice were sacrificed and lung sections were used for H&E staining. Representative lung tissues from surviving and naïve mice are shown. Scale bar, 100 μm.

in vivo, we compared the therapeutic efficacies of 1H3 and its Fab, which cannot mediate ADCC. Mice treated with Fab had significantly fewer lung tumor nodules than did mice treated with control IgG, but they had significantly more lung tumor nodules than did mice treated with 1H3 (Figure 5C). To confirm this effect, we validated the efficacy of 1H3 and Fab of 1H3 on the primary tumor model of B7x/4T1. 1H3 showed superior efficacy to that of 1H3 Fab (Figure S4B). Taken together, these results suggest that 1H3 inhibits tumor growth through the combination of ADCC and functional neutralization of B7x.

DISCUSSION

Here, we solved the structure of the functional IgV domain of B7x and developed a cancer immunotherapy targeting B7x. The B7 and CD28 families are very attractive therapeutic targets for human cancers. Compared to CTLA-4, PD-1, and PD-L1, which are targets for current clinical trials (Brahmer et al., 2012; Topalian et al., 2012), B7x has a very different expression pattern. In humans, CTLA-4, PD-1, and PD-L1 are not expressed on resting T cells, but they are induced after T cell activation and expressed on Tregs (Scandiuzzi et al., 2011). PD-1 and PD-L1 are induced on B cells, monocytes, and other immune cells after stimulation. By contrast, human B7x is hardly detected on immune cells even after stimulation (Lee et al., 2012). Neither CTLA-4 nor PD-1 are expressed on nonhematopoietic cells. PD-L1 is expressed on some normal tissues, whereas B7x is hardly detected in most human tissues (Choi et al., 2003). PD-L1 is expressed in some human cancers (Zang and Allison, 2007), whereas the expression of B7x in human cancers is more extensive, including cancers of the esophagus (Chen et al., 2011), lung (Sun et al., 2006), breast (Tringler et al., 2005), pancreas (Awadallah et al., 2008), kidney (Krambeck et al., 2006), gut (Jiang et al., 2010), skin (Quandt et al., 2011), ovary (Zang et al., 2010), and prostate (Zang et al., 2007). Therefore, the expression pattern of B7x suggests that this target is more cancer specific.

The overall organization of the human B7x IgV domain is similar to that of other B7 family members (e.g., a structural alignment with PD-L1 is shown in Figure 1C). In addition to the secondary structure topology, conserved features include the disulfide bond connecting strands B and F (formed by Cys56 and Cys130) and the tryptophan residue (Trp71) at the domain core. The receptor-binding interface described for other B7 family members is located on the front-sheet surface of their IgV domains (Lázár-Molnár et al., 2008; Schwartz et al., 2001; Stamper et al., 2001). Thus, it is likely that B7x engages its receptor on the equivalent surface. Furthermore, our observation of a large branched glycan of the back sheet of the B7x-IgV (linked to Asn112) would suggest that the back-sheet surface is unlikely to participate in receptor recognition. A glycosylation site at an equivalent position has been previously reported for the murine B7-H3 ectodomain (Vigdorovich et al., 2013).

We demonstrated that mAbs against B7x achieved significant therapeutic efficacy in mouse cancer models. A new study also demonstrates that the anti-B7x single-chain fragments variable (scFv) can delay OVCAR5 line growth in NSG mice (Dangaj et al., 2013). We and other groups have previously shown that activated T cells express an unidentified receptor for B7x (Prasad et al., 2003; Sica et al., 2003; Zang et al., 2003), and our recent work reveals that MDSCs also have a receptor for B7x (Abadi et al., 2013). These results suggest that the expression of the B7x receptors is broader than previously thought. Due to the lack of the identity of B7x receptors, we developed an in vivo functional screen for anti-B7x mAbs. We found that the expression of B7x on CT26 tumor cells significantly promoted tumor progression in vivo, which mirrored clinical observations, and was used to validate therapeutic mAbs. 1H3 and 12D11 were found to reduce more than 60% of tumor nodules in lungs, with development of a strong immunologic memory in the case of 1H3. Similar results were obtained with the 4T1 tumor model.

Characterization of 1H3's binding properties showed that in addition to recognizing murine B7x, it also bound strongly to the IgV domain of human B7x and was able to significantly inhibit tumor nodule formation of human B7x-expressing CT26 in lungs. These results suggest that humanized 1H3 may prove useful in the treatment of human cancers. To advance this strategy, we mapped the epitopes recognized by 1H3 on human B7x using a series of mutants whose design was guided by the structure of B7x-IgV. The clustering of the antibody-blocking mutants to the "top" of the molecule, in particular, residues Ile62 and Lys63 in the BC loop of the back sheet and residue Ser135 in the FG loop of the front sheet, defines the minimal footprint for the B7x:1H3 binding interface. The combination of 1H3 functional blocking data and the mutagenesis data suggests that the binding surface for the physiologically relevant B7x receptor partially overlaps with this surface. Our results are consistent with observations that IgV domains predominantly interact with other IgV domains via strands and a loop on their front sheets like is seen in the interactions between CTLA-4 and PD-1 and their ligands (Figures S5A–S5D).
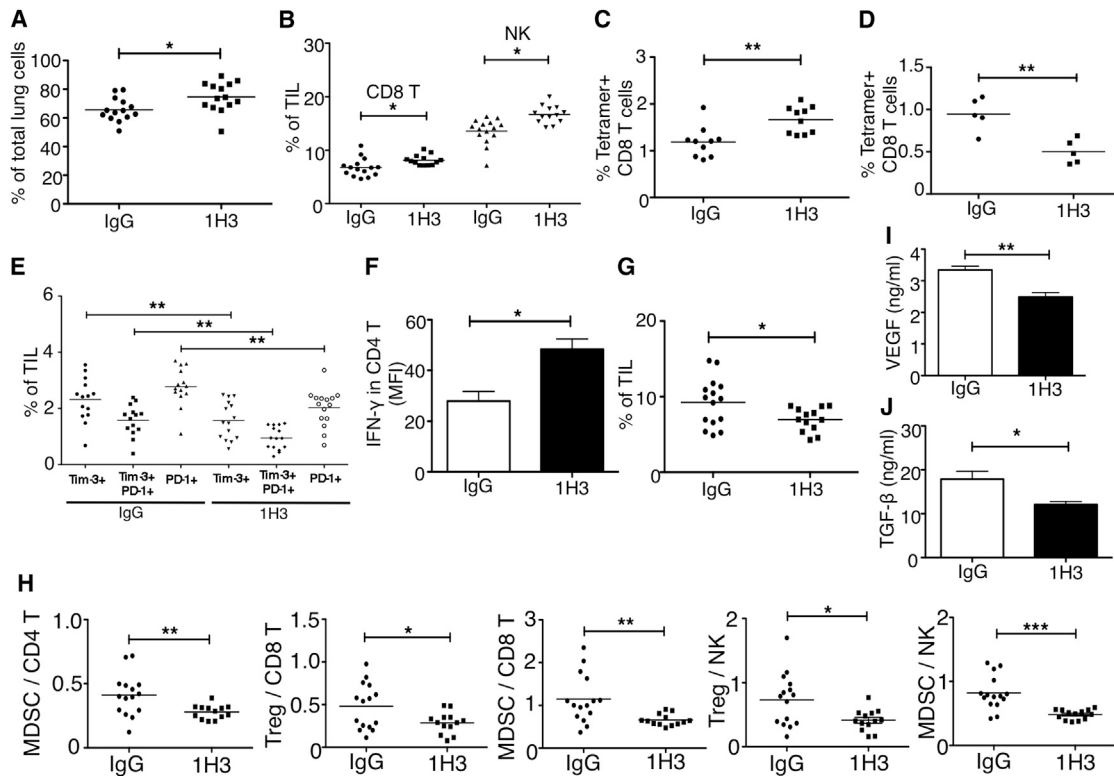
Figure 4. Anti-B7x Therapy Alters the Intratumor Balance of Antitumor Effector Immune Cells and Immunosuppressive Cells

(A–G) BALB/c mice were i.v. injected with B7x/CT26 and then treated with 1H3 or control mouse IgG. At day 17, single-cell suspensions from tumor-bearing lungs were analyzed by FACS for the percentage of infiltrated CD45+ cells (A), the percentage of CD8 T cells and NK cells (B), the percentage of tumor antigen AH1 (SPSYVYHQF)-specific CD8 T cells (C), the percentage of CD4 T cells that were Tim-3+PD-1+, Tim-3+ alone and PD-1+ alone (E), and CD11b+Ly6C+ monocytic myeloid-derived suppressor cells (G). At day 17, single-cell suspensions from blood were analyzed by FACS for the percentage of tumor antigen AH1-specific CD8+ T cells were measured (D). Cell suspensions from tumor-bearing lungs were stimulated with 1× cell stimulation cocktail for 5 hr and stained with antibodies to CD3, CD4 and IFN-γ or isotype controls (F). Results are pooled from three independent experiments; *p < 0.05, **p < 0.01. Result in (D) is representative of data from two independent experiments.

(H) The ratios of Treg (Foxp3+CD4+) and MDSCs to CD8 T cells, CD4 T cells, and NK cells. These results are pooled from three independent experiments; *p < 0.05, **p < 0.01, ***p < 0.001.

(I) Total amount of VEGF from tumor-bearing lungs was measured using ELISA. **p < 0.01.

(J) Total amount of TGF-β from tumor-bearing lungs was measured using ELISA. Each group contained five mice. *p < 0.05.

It is surprising that 1H3 and 12D11 recognized similar epitopes in human B7x, because 12D11 showed no in vivo suppressive effect on human B7x-expressing CT26 cells. However, even though the difference was minor, 1H3 and 12D11 had at least one difference. Ile62's position in the IgV domain of human B7x seemed to play a significant role in the binding of B7x and anti-B7x mAbs. These results highlight the importance of our in vivo screening system to find therapeutic mAbs against B7x.

The studies presented here suggest that the principal mechanisms of the anti-B7x mAb in dampening tumor progression are the neutralization of the B7x-mediated coinhibition of T cells and the ADCC-mediated direct killing of tumor cells. We demonstrated that 1H3 killed B7x-expressing tumor cells in a dose-dependent manner and that both 1H3 and its Fab fragment partially recovered T cell proliferation suppressed by B7x-Ig fusion protein. In line with these results, the Fab treatment significantly reduced lung tumor nodules, but its therapeutic efficacy was not as great as full 1H3 mAb treatment. These results sug-

gest that both neutralization and ADCC may take place in vivo during the 1H3 treatment. The 1H3 treatment strongly increased the infiltration of major types of antitumor immune cells such as CD8 T cells including tumor antigen-specific CD8 T cells, NK cells, and IFN-γ-producing CD4 T cells. On the other hand, the treatment markedly reduced infiltration of immunosuppressive MDSCs. As a consequence, the treatment shifted the tumor microenvironment to a favorable antitumor state with a significantly higher ratio of effector immune cells to the suppressive MDSCs and Tregs. Correspondingly, we found less VEGF and TGF-β in the tumor microenvironment after 1H3 treatment.

Therapies with mAbs against CTLA-4 and PD-1 target T cell coinhibitory receptors, whereas therapies with mAbs against PD-L1 and B7x target T cell coinhibitory ligands. The encouraging safety profile and antitumor activity from an anti-PD-L1 clinical trial (Brahmer et al., 2012), together with preliminary data from an anti-PD-1 trial that have suggested a correlation between tumor membrane PD-L1 expression and clinical response
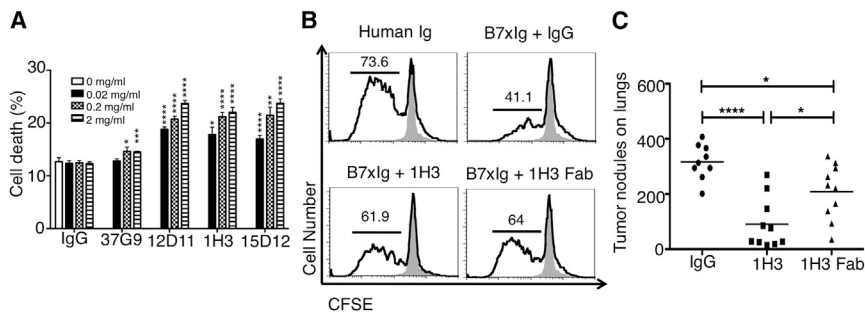
Figure 5. Antitumor Mechanisms of 1H3 Treatment

(A) mAbs against B7x killed CT26 tumor cells expressing B7x through antibody-dependent cellular cytotoxicity in vitro. Data are representative of two independent experiments in triplicates and shown as mean ± SE. **p < 0.01; ****p < 0.0001.

(B) 1H3 partially neutralized B7x-mediated T cell coinhibition. CFSE-labeled T cells were incubated for four days with plate-bound anti-CD3 in the presence of control Ig, B7x-Ig and IgG (2 μg/ml), B7x-Ig and 1H3 (2 μg/ml), or B7x-Ig and 1H3 Fab (4 μg/ml). Representative FACS plots show CFSE dilution among live stimulated cells (solid line) compared to unstimulated control T cells (shaded area). Data are representative of two independent experiments. (C) Comparison of therapeutic efficacies between 1H3 and its Fab. Data were pooled from two independent experiments (n = 9 or 10). *p < 0.05; **p < 0.01; ***p < 0.001; ****p < 0.0001.

to anti-PD-1 antibodies (Topalian et al., 2012), highlight the emerging significance of targeting coinhibitory B7 ligands. Further studies with humanized anti-B7x antibodies, either as monotherapy or in synergism with traditional therapies, should be pursued for the treatment of human cancers.

EXPERIMENTAL PROCEDURES

Protein Crystallization and Structure Determination

Purified human B7x IgV protein was concentrated to 10 mg/ml in HBS-E (10 mM HEPES [pH 7], 150 mM NaCl, 1 mM EDTA) and used to determine the initial crystallization conditions. Diffraction-quality crystals were obtained in 200 mM tripotassium citrate, 2.2 M ammonium sulfate, soaked in the well solution supplemented with 5-amino-2,4,6 triiodoisophthalic acid monohydrate (I3C) (Hampton Research) as a phasing reagent and 400 mM (final volume) lithium sulfate and flash-cooled in liquid nitrogen. Data sets at 1.075 Å and 1.54 Å wavelength were collected at the National Synchrotron Light Source beamline X29 (Upton, NY). Data were integrated using the iMosflm (Battye et al., 2011) with subsequent processing using the programs within the CCP4 software package (Winn et al., 2011). Single-wavelength anomalous dispersion (SAD) phasing was carried out using the anomalous iodine (I3C) signal from a data set collected at 1.54 Å, and the initial electron density maps were obtained using SHELXC/D/E (Sheldrick, 2008) and HKL2MAP. Following initial model building using ARP/wARP (Langer et al., 2008), the model was refined using REFMAC5 (Murshudov et al., 1997) with further manual building using Coot (Emsley et al., 2010).

Animals and Human Tissue Slides

BALB/c mice were purchased from the National Cancer Institute and The Jackson Laboratory. All mice were housed in a specific-pathogen-free facility. Human tumor tissue sections were obtained from IMEGENEX. All protocols were reviewed and approved by the Albert Einstein College of Medicine Institutional Animal Care and Use Committee and Institutional Review Board.

Monoclonal Antibodies against B7x and Generation of Fab Fragment

Hybridoma cells from 37G9, 12D11, 1H3, and 15D12 clones were maintained in serum-free RPMI-1640 media (Wei et al., 2011). mAbs were purified on a Protein G column (Thermo Scientific). Fractions of eluted mAbs were measured and pooled for buffer exchange to PBS via dialysis. Fab fragment preparation was performed based on the manufacturer's protocol (Thermo Scientific).

Cell Lines and Tumors

CT26 and B7x/CT26 were cultured in RPMI-1640 containing 10% fetal bovine serum (FBS), 100 U/ml penicillin, 100 μg/ml streptomycin, 2 mM L-glutamine, 1% nonessential amino acids, and 1 mM sodium pyruvate. 4T1 and B7x/4T1 were cultured in Dulbecco's modified Eagle's medium (DMEM) supplemented with 10% FBS and 0.4 U/ml insulin as described previously (Abadi et al., 2013).

The 8- to 10-week-old mice were i.v. injected with 10^5 cells in 0.2 ml DMEM. For survival studies of CT26 and B7x/CT26, 10^5 B7x/CT26 cells were i.v. injected into mice and survival rate was examined. For survival studies of 1H3 treatment, 10^4 B7x/CT26 cells were i.v. injected into mice, and the same numbers of B7x/CT26 cells were injected for rechallenge. For the primary tumor experiment, 10^5 B7x/4T1 cells were injected subcutaneously into the mammary fat pad of female mice. Tumor nodules on lungs were measures as previously described (Abadi et al., 2013).

Anti-B7x Immunotherapy

A total of 200 μg of mAbs against B7x, 1H3 Fab, or normal mouse IgG were i.p. injected at days 1, 3, 7, 11, and 14. Each mouse received a total of 1 mg of antibody or Fab during B7x/CT26 experiments. At day 17, mice were sacrificed for counting tumor nodules in lungs. For hB7x/CT26 experiments, 200 μg of mAbs against B7x (1H3 and 12D11) or normal mouse IgG was i.p. injected at days 1, 2, 3, 5, 7, 9, 11, 13, and 15. Each mouse received a total of 1.8 mg antibody. At day 17, mice were sacrificed for counting tumor nodules in lungs. For the B7x/4T1 primary tumor model, 1 week after tumor injection, mice were grouped based on their tumor volume. A total of 300 μg of mAbs was i.p. injected at days 8, 11, 13, 15, and 18. Tumor volume was measured every 2 or 3 days after 7 days. At day 20, mice were sacrificed, breast tumors were excised and weighed, and tumor nodules on lungs were counted.

Human B7x Mutagenesis and Epitope Mapping

Ectodomain of hB7x (Gly21-Ala208) was cloned into a type I secretion ligation independent cloning vector we designed in house. Cloning into this vector fuses the target ectodomain to a nonnative transmembrane domain (TM domain from murine PD-L1) followed by the mCherry protein (as a cytosolic expression proxy). We have successfully used this vector to study expression, localization, and activity of several other members of the IgG superfamily. The wild-type hB7x type I secretion construct was transfected into human embryonic kidney 293S (HEK293S) cells. Cell-surface expression of B7x was confirmed by fluorescence-activated cell sorting (FACS) analysis using the B7x-specific mAb 1H3. Residues for site-directed mutagenesis were initially selected on the basis of our crystal structure of the hB7x-IgV domain to identify surface-exposed residues within the IgV domain. Surface-exposed residues clearly involved in a salt bridge were omitted from the set of targeted residues. Mutagenesis was performed using a standard PCR method using high-fidelity KOD polymerase. All of the successful mutants were sequence-verified and individually transfected into HEK293S cells using 24-well suspension plates. Two days posttransfection, the cells were counted and diluted to 1×10^6 cells/ml using 1× PBS with 2% BSA. A total of 0.2×10^6 cells were incubated with 2 μg of the 1H3 mAb for 1 hr at 4°C. Cells were subsequently pelleted by centrifugation at 500 × g and washed with PBS for a total of three times. Goat anti-mouse DyLight 488 secondary antibody (2 μg) was added to the cells, and they were incubated at 4°C for 45 min. Cells were washed, and antibody binding was assessed by FACS analysis on a BD Aria III. Flow cytometry data were gated for all mCherry-positive events (hB7x expression) and then subgated for anti-B7x binding (488 channel). To consider slight variation in total expression

of each mutant, the number of antibody-bound events was divided by the total number of mCherry-positive events. The experiment was performed in duplicate.

Statistics

Statistical analysis was performed with Prism software (GraphPad) using the unpaired Student's t test or the log-rank test (Mantel-Cox) for the survival study. p values < 0.05 were considered statistically significant.

Other detailed experimental procedures can be found in the Supplemental Experimental Procedures.

ACCESSION NUMBERS

Final coordinates and structure factors were deposited in Protein Data Bank and are available under accession number 4GOS.

SUPPLEMENTAL INFORMATION

Supplemental Information includes Supplemental Experimental Procedures and five figures and can be found with this article online at http://dx.doi.org/10.1016/j.celrep.2014.09.053.

AUTHOR CONTRIBUTIONS

H.J. performed experiments in immunotherapy. V.V. and U.A.R. determined the crystal structure. V.V. performed the affinity measurements. S.C.G performed epitope mapping. M.J. performed immunohistochemistry experiments. Y.M.A. helped with several experiments. J.S.L. established cell lines. L.S., K.C.O., J.M.C., R.Z., Y.Y., Y.M., and J.A.S. provided invaluable reagents and advice on experiments. H.J. and V.V. analyzed the data and wrote the manuscript. X.Z. and S.C.A. supervised the study and wrote the manuscript. All authors read and approved the manuscript.

ACKNOWLEDGMENTS

REFERENCES

Abadi, Y.M., Jeon, H., Ohaegbulam, K.C., Scandiuzzi, L., Ghosh, K., Hofmeyer, K.A., Lee, J.S., Ray, A., Gravekamp, C., and Zang, X. (2013). Host b7x promotes pulmonary metastasis of breast cancer. J. Immunol. 190, 3806–3814.

Aslakson, C.J., and Miller, F.R. (1992). Selective events in the metastatic process defined by analysis of the sequential dissemination of subpopulations of a mouse mammary tumor. Cancer Res. 52, 1399–1405.

Awadallah, N.S., Shroyer, K.R., Langer, D.A., Torkko, K.C., Chen, Y.K., Bentz, J.S., Papkoff, J., Liu, W., Nash, S.R., and Shah, R.J. (2008). Detection of B7-H4 and p53 in pancreatic cancer: potential role as a cytological diagnostic adjunct. Pancreas 36, 200–206.

Barach, Y.S., Lee, J.S., and Zang, X. (2011). T cell coinhibition in prostate cancer: new immune evasion pathways and emerging therapeutics. Trends Mol. Med. 17, 47–55.

Battye, T.G., Kontogiannis, L., Johnson, O., Powell, H.R., and Leslie, A.G. (2011). iMOSFLM: a new graphical interface for diffraction-image processing with MOSFLM. Acta Crystallogr. D Biol. Crystallogr. 67, 271–281.

Brahmer, J.R., Tykodi, S.S., Chow, L.Q., Hwu, W.J., Topalian, S.L., Hwu, P., Drake, C.G., Camacho, L.H., Kauh, J., Odunsi, K., et al. (2012). Safety and activity of anti-PD-L1 antibody in patients with advanced cancer. N. Engl. J. Med. 366, 2455–2465.

Chen, L.J., Sun, J., Wu, H.Y., Zhou, S.M., Tan, Y., Tan, M., Shan, B.E., Lu, B.F., and Zhang, X.G. (2011). B7-H4 expression associates with cancer progression and predicts patient's survival in human esophageal squamous cell carcinoma. Cancer Immunol. Immunother. 60, 1047–1055.

Choi, I.H., Zhu, G., Sica, G.L., Strome, S.E., Cheville, J.C., Lau, J.S., Zhu, Y., Flies, D.B., Tamada, K., and Chen, L. (2003). Genomic organization and expression analysis of B7-H4, an immune inhibitory molecule of the B7 family. J. Immunol. 171, 4650–4654.

Clynes, R.A., Towers, T.L., Presta, L.G., and Ravetch, J.V. (2000). Inhibitory Fc receptors modulate in vivo cytotoxicity against tumor targets. Nat. Med. 6, 443–446.

Dangaj, D., Lanitis, E., Zhao, A., Joshi, S., Cheng, Y., Sandaltzopoulos, R., Ra, H.J., Danet-Desnoyers, G., Powell, D.J., Jr., and Scholler, N. (2013). Novel recombinant human b7-h4 antibodies overcome tumoral immune escape to potentiate T-cell antitumor responses. Cancer Res. 73, 4820–4829.

Emsley, P., Lohkamp, B., Scott, W.G., and Cowtan, K. (2010). Features and development of Coot. Acta Crystallogr. D Biol. Crystallogr. 66, 486–501.

Fiocco, U., Sfriso, P., Oliviero, F., Pagnin, E., Scagliori, E., Campana, C., Dainese, S., Cozzi, L., and Punzi, L. (2008). Co-stimulatory modulation in rheumatoid arthritis: the role of (CTLA4-Ig) abatacept. Autoimmun. Rev. 8, 76–82.

Fourcade, J., Sun, Z., Benallaoua, M., Guillaume, P., Luescher, I.F., Sander, C., Kirkwood, J.M., Kuchroo, V., and Zarour, H.M. (2010). Upregulation of Tim-3 and PD-1 expression is associated with tumor antigen-specific CD8+ T cell dysfunction in melanoma patients. J. Exp. Med. 207, 2175–2186.

Fridlender, Z.G., Sun, J., Kim, S., Kapoor, V., Cheng, G., Ling, L., Worthen, G.S., and Albelda, S.M. (2009). Polarization of tumor-associated neutrophil phenotype by TGF-beta: "N1" versus "N2" TAN. Cancer Cell 16, 183–194.

Goding, S.R., Wilson, K.A., Xie, Y., Harris, K.M., Baxi, A., Akpinarli, A., Fulton, A., Tamada, K., Strome, S.E., and Antony, P.A. (2013). Restoring immune function of tumor-specific CD4+ T cells during recurrence of melanoma. J. Immunol. 190, 4899–4909.

Greenwald, R.J., Freeman, G.J., and Sharpe, A.H. (2005). The B7 family revisited. Annu. Rev. Immunol. 23, 515–548.

Hodi, F.S., O'Day, S.J., McDermott, D.F., Weber, R.W., Sosman, J.A., Haanen, J.B., Gonzalez, R., Robert, C., Schadendorf, D., Hassel, J.C., et al. (2010). Improved survival with ipilimumab in patients with metastatic melanoma. N. Engl. J. Med. 363, 711–723.

Hofmeyer, K.A., Scandiuzzi, L., Ghosh, K., Pirofski, L.A., and Zang, X. (2012). Tissue-expressed B7x affects the immune response to and outcome of lethal pulmonary infection. J. Immunol. 189, 3054–3063.

Huang, A.Y., Gulden, P.H., Woods, A.S., Thomas, M.C., Tong, C.D., Wang, W., Engelhard, V.H., Pasternack, G., Cotter, R., Hunt, D., et al. (1996). The immunodominant major histocompatibility complex class I-restricted antigen of a murine colon tumor derives from an endogenous retroviral gene product. Proc. Natl. Acad. Sci. USA 93, 9730–9735.

Isitman, G., Stratov, I., and Kent, S.J. (2012). Antibody-dependent cellular cytotoxicity and NK cell-driven immune escape in HIV infection: implications for HIV vaccine development. Adv. Virol. 2012, 637208.

Janakiram, M., Abadi, Y.M., Sparano, J.A., and Zang, X. (2012). T cell coinhibition and immunotherapy in human breast cancer. Discov. Med. 14, 229–236.

Jeon, H., Ohaegbulam, K.C., Abadi, Y.M., and Zang, X. (2013). B7x and myeloid-derived suppressor cells in the tumor microenvironment: A tale of two cities. OncoImmunology 2, e24744.

Jiang, J., Zhu, Y., Wu, C., Shen, Y., Wei, W., Chen, L., Zheng, X., Sun, J., Lu, B., and Zhang, X. (2010). Tumor expression of B7-H4 predicts poor survival of patients suffering from gastric cancer. Cancer Immunol. Immunother. 59, 1707–1714.

Kohrt, H.E., Houot, R., Marabelle, A., Cho, H.J., Osman, K., Goldstein, M., Levy, R., and Brody, J. (2012). Combination strategies to enhance antitumor ADCC. Immunotherapy 4, 511–527.

Krambeck, A.E., Thompson, R.H., Dong, H., Lohse, C.M., Park, E.S., Kuntz, S.M., Leibovich, B.C., Blute, M.L., Cheville, J.C., and Kwon, E.D. (2006). B7-H4 expression in renal cell carcinoma and tumor vasculature: associations with cancer progression and survival. Proc. Natl. Acad. Sci. USA 103, 10391–10396.

Langer, G., Cohen, S.X., Lamzin, V.S., and Perrakis, A. (2008). Automated macromolecular model building for X-ray crystallography using ARP/wARP version 7. Nat. Protoc. 3, 1171–1179.

Lázár-Molnár, E., Yan, Q., Cao, E., Ramagopal, U., Nathenson, S.G., and Almo, S.C. (2008). Crystal structure of the complex between programmed death-1 (PD-1) and its ligand PD-L2. Proc. Natl. Acad. Sci. USA 105, 10483–10488.

Lee, J.S., Scandiuzzi, L., Ray, A., Wei, J., Hofmeyer, K.A., Abadi, Y.M., Loke, P., Lin, J., Yuan, J., Serreze, D.V., et al. (2012). B7x in the periphery abrogates pancreas-specific damage mediated by self-reactive CD8 T cells. J. Immunol. 189, 4165–4174.

Lin, D.Y., Tanaka, Y., Iwasaki, M., Gittis, A.G., Su, H.P., Mikami, B., Okazaki, T., Honjo, T., Minato, N., and Garboczi, D.N. (2008). The PD-1/PD-L1 complex resembles the antigen-binding Fv domains of antibodies and T cell receptors. Proc. Natl. Acad. Sci. USA 105, 3011–3016.

Murshudov, G.N., Vagin, A.A., and Dodson, E.J. (1997). Refinement of macromolecular structures by the maximum-likelihood method. Acta Crystallogr. D Biol. Crystallogr. 53, 240–255.

Prasad, D.V., Richards, S., Mai, X.M., and Dong, C. (2003). B7S1, a novel B7 family member that negatively regulates T cell activation. Immunity 18, 863–873.

Quandt, D., Fiedler, E., Boettcher, D., Marsch, W.Ch., and Seliger, B. (2011). B7-h4 expression in human melanoma: its association with patients' survival and antitumor immune response. Clin. Cancer Res. 17, 3100–3111.

Roda, J.M., Wang, Y., Sumner, L.A., Phillips, G.S., Marsh, C.B., and Eubank, T.D. (2012). Stabilization of HIF-2α induces sVEGFR-1 production from tumor-associated macrophages and decreases tumor growth in a murine melanoma model. J. Immunol. 189, 3168–3177.

Roland, C.L., Lynn, K.D., Toombs, J.E., Dineen, S.P., Udugamasooriya, D.G., and Brekken, R.A. (2009). Cytokine levels correlate with immune cell infiltration after anti-VEGF therapy in preclinical mouse models of breast cancer. PLoS ONE 4, e7669.

Scandiuzzi, L., Ghosh, K., and Zang, X. (2011). T cell costimulation and coinhibition: genetics and disease. Discov. Med. 12, 119–128.

Schwartz, J.C., Zhang, X., Fedorov, A.A., Nathenson, S.G., and Almo, S.C. (2001). Structural basis for co-stimulation by the human CTLA-4/B7-2 complex. Nature 410, 604–608.

Sharma, P., Wagner, K., Wolchok, J.D., and Allison, J.P. (2011). Novel cancer immunotherapy agents with survival benefit: recent successes and next steps. Nat. Rev. Cancer 11, 805–812.

Sheldrick, G.M. (2008). A short history of SHELX. Acta Crystallogr. A 64, 112–122.

Sica, G.L., Choi, I.H., Zhu, G., Tamada, K., Wang, S.D., Tamura, H., Chapoval, A.I., Flies, D.B., Bajorath, J., and Chen, L. (2003). B7-H4, a molecule of the B7 family, negatively regulates T cell immunity. Immunity 18, 849–861.

Stamper, C.C., Zhang, Y., Tobin, J.F., Erbe, D.V., Ikemizu, S., Davis, S.J., Stahl, M.L., Seehra, J., Somers, W.S., and Mosyak, L. (2001). Crystal structure of the B7-1/CTLA-4 complex that inhibits human immune responses. Nature 410, 608–611.

Sun, Y., Wang, Y., Zhao, J., Gu, M., Giscombe, R., Lefvert, A.K., and Wang, X. (2006). B7-H3 and B7-H4 expression in non-small-cell lung cancer. Lung Cancer 53, 143–151.

Topalian, S.L., Hodi, F.S., Brahmer, J.R., Gettinger, S.N., Smith, D.C., McDermott, D.F., Powderly, J.D., Carvajal, R.D., Sosman, J.A., Atkins, M.B., et al. (2012). Safety, activity, and immune correlates of anti-PD-1 antibody in cancer. N. Engl. J. Med. 366, 2443–2454.

Tringler, B., Zhuo, S., Pilkington, G., Torkko, K.C., Singh, M., Lucia, M.S., Heinz, D.E., Papkoff, J., and Shroyer, K.R. (2005). B7-h4 is highly expressed in ductal and lobular breast cancer. Clin. Cancer Res. 11, 1842–1848.

Vigdorovich, V., Ramagopal, U.A., Lázár-Molnár, E., Sylvestre, E., Lee, J.S., Hofmeyer, K.A., Zang, X., Nathenson, S.G., and Almo, S.C. (2013). Structure and T cell inhibition properties of B7 family member, B7-H3. Structure 21, 707–717.

Vincenti, F., Dritselis, A., and Kirkpatrick, P. (2011). Belatacept. Nat. Rev. Drug Discov. 10, 655–656.

Wei, J., Loke, P., Zang, X., and Allison, J.P. (2011). Tissue-specific expression of B7x protects from CD4 T cell-mediated autoimmunity. J. Exp. Med. 208, 1683–1694.

Winn, M.D., Ballard, C.C., Cowtan, K.D., Dodson, E.J., Emsley, P., Evans, P.R., Keegan, R.M., Krissinel, E.B., Leslie, A.G., McCoy, A., et al. (2011). Overview of the CCP4 suite and current developments. Acta Crystallogr. D Biol. Crystallogr. 67, 235–242.

Zang, X., and Allison, J.P. (2007). The B7 family and cancer therapy: costimulation and coinhibition. Clin. Cancer Res. 13, 5271–5279.

Zang, X., Loke, P., Kim, J., Murphy, K., Waitz, R., and Allison, J.P. (2003). B7x: a widely expressed B7 family member that inhibits T cell activation. Proc. Natl. Acad. Sci. USA 100, 10388–10392.

Zang, X., Thompson, R.H., Al-Ahmadie, H.A., Serio, A.M., Reuter, V.E., Eastham, J.A., Scardino, P.T., Sharma, P., and Allison, J.P. (2007). B7-H3 and B7x are highly expressed in human prostate cancer and associated with disease spread and poor outcome. Proc. Natl. Acad. Sci. USA 104, 19458–19463.

Zang, X., Sullivan, P.S., Soslow, R.A., Waitz, R., Reuter, V.E., Wilton, A., Thaler, H.T., Arul, M., Slovin, S.F., Wei, J., et al. (2010). Tumor associated endothelial expression of B7-H3 predicts survival in ovarian carcinomas. Mod. Pathol. 23, 1104–1112.

Zhao, R., Chinai, J.M., Buhl, S., Scandiuzzi, L., Ray, A., Jeon, H., Ohaegbulam, K.C., Ghosh, K., Zhao, A., Scharff, M.D., and Zang, X. (2013). HHLA2 is a member of the B7 family and inhibits human CD4 and CD8 T-cell function. Proc. Natl. Acad. Sci. USA 110, 9879–9884.

Zhou, Q., Munger, M.E., Veenstra, R.G., Weigel, B.J., Hirashima, M., Munn, D.H., Murphy, W.J., Azuma, M., Anderson, A.C., Kuchroo, V.K., and Blazar, B.R. (2011). Coexpression of Tim-3 and PD-1 identifies a CD8+ T-cell exhaustion phenotype in mice with disseminated acute myelogenous leukemia. Blood 117, 4501–4510.

Zhu, Y., Yao, S., Iliopoulou, B.P., Han, X., Augustine, M.M., Xu, H., Phennicie, R.T., Flies, S.J., Broadwater, M., Ruff, W., et al. (2013). B7-H5 costimulates human T cells via CD28H. Nat Commun 4, 2043.